JOURNAL OF MATERIALS SCIENCE 10 (1975) 1323–1333

Deformation of a carbon–epoxy composite under hydrostatic pressure

C. W. WEAVER, J. G. WILLIAMS
Materials Research Laboratories, Melbourne, Australia

This paper describes the behaviour of a carbon-fibre reinforced epoxy composite when deformed in compression under high hydrostatic confining pressures. The composite consisted of 36% by volume of continuous fibres of Modmur Type II embedded in Epikote 828 epoxy resin. When deformed under pressures of less than 100 MPa the composite failed by longitudinal splitting, but splitting was suppressed at higher pressures (up to 500 MPa) and failure was by kinking. The failure strength of the composite increased rapidly with increasing confining pressure, though the elastic modulus remained constant. This suggests that the pressure effects were introduced by fracture processes. Microscopical examination of the kinked structures showed that the carbon fibres in the kink bands were broken into many fairly uniform short lengths. A model for kinking in the composite is suggested which involves the buckling and fracture of the carbon fibres.

List of symbols

d	diameter of fibre
E_f	elastic modulus of fibre
E_m	elastic modulus of epoxy
G_m	shear modulus of epoxy
k	radius of gyration of fibre section
l	length of buckle in fibre
P	confining pressure ($= \sigma_2 = \sigma_3$)
R	radius of bent fibre
V_f	volume fraction of fibres in composite
ϵ_t, ϵ_c	bending strains in fibres
θ	angle between the plane of fracture and σ_1
σ_1	principal stress
σ_3	confining pressure
σ_c	strength of composite
σ_f	strength of fibre in buckling mode
σ_n	normal stress on a fracture plane
σ_m	strength of epoxy matrix
τ	shear stress
ϕ	tangent slope of Mohr envelope
ψ	slope of pressure versus strength curves in Figs. 3 and 4.

1. Introduction

The strength of fibre-reinforced composites when loaded in compression parallel to the fibre axis is usually limited by the transverse strength of the matrix or of the fibre-matrix interface, following buckling of the fibres under load [1, 2]. The mode of failure depends on both the properties of the fibre and the matrix and may take the form of fibre buckling, transverse deformation bands or cracking and debonding of the fibres [3, 4]. In the carbon-epoxy material studied, failure at atmospheric pressure usually occurred by longitudinal splitting, but this can be prevented by conducting the tests in a high pressure environment, in which case the hydrostatic compressive forces will suppress fracturing so that other kinds of deformation may develop.

Under high confining pressures, the mode of failure changed from longitudinal splitting to kinking in zones lying at a high angle to the principal stress axis, and the failure strength of the composite increased rapidly as pressure was increased. A model for kinking in the composite is proposed, stress calculations suggesting that the kinking was initiated by the fracturing of buckled fibres.

2. Experimental

2.1. Preparation of specimens

The matrix used was a commercial epoxy resin based on the diglycidyl ether of 2,2-bis (4′-hydroxy phenyl)-propane (Epikote 828 from Shell Chemical Australia Pty Ltd.) It was cured with the stoichiometric quantity of laboratory grade 1,3 diaminopropane (from Aldrich Chemicals). The reinforcement was surface-treated high strength carbon fibre (Modmur, type II).

The composite was prepared by wetting an appropriate weight of fibre with resin and

pulling it into a metal tube lined with a thin-walled teflon tube. The samples were cured for 20 h at 60°C and postcured for 200 min at 150°C. The samples were calculated to have 36% volume fraction of carbon. These provided three rods (A, B and C) measuring approximately 5 mm diameter and 200 mm long.

The alignment of the carbon fibre in the composites was by no means ideal and their distribution through the samples was not uniform. These specimens did not, therefore, represent the condition of maximum strength and uniformity for the composite, and some scatter of experimental results probably resulted. Details of their microstructure will be described later.

2.2. High pressure apparatus

The high pressure straining apparatus was designed by Heard [5], and was capable of applying axial strains in compression under hydrostatic pressures up to 500 MPa, or occasionally up to 650 MPa, using ethyl alcohol as the confining fluid. The differential axial load on the specimen was measured directly by an internal force gauge column and the applied axial strain was measured from the movement of the deforming piston. Continuous autographic records of the forces and strains applied during deformation were thus obtained throughout the tests.

The carbon-epoxy specimens were sealed in annealed copper jackets 0.25 mm thick and 10 mm diameter before being deformed, in order to prevent ingress of the high pressure confining fluid which could cause premature failure. The space between the specimen and the copper jacket was filled with a natural rubber sleeve [5]. The copper jackets were sealed onto the loading pistons by means of hardened steel rings as described by Paterson [6]. In view of the high strength of the composite specimens, the forces required to deform the copper and rubber jackets were considered negligible.

For compression testing, specimens 10 to 12 mm long were cut from the rods and the ends carefully ground flat and parallel and normal to the longitudinal axis. Straining in compression was applied to the specimens, after pressurizing to the desired level, at a strain rate of 0.125 mm min^{-1} (i.e. at a rate of approximately 0.01 min^{-1}).

3. Experimental results

3.1. Deformation of carbon–epoxy specimens

When deformed in compression at atmospheric pressure, the carbon-epoxy specimens invariably failed by longitudinal splitting and break-up of the ends, but under moderate confining pressures the splitting was contained and deformation occurred locally in bands across the specimens. These changes in the morphology of failure are shown in Fig. 1. The deformation bands were sometimes associated with transverse cracking but, at the highest pressure, quite complex deformation occurred which was found to consist of complex multiple kinking.

A number of typical force-displacement curves for rod A, as recorded during the tests, are shown in Fig. 2. These are characterized by two features:

(a) after a period of elastic deformation, failure or deformation always occurred abruptly with a large drop in load. Further deformation then occurred at constant load;

(b) strength increased considerably with increased confining pressure; the level of load at which the post-yield deformation continued also generally increased with pressure.

Evidence of some small amounts of deformation preceding the drop in load was also recorded, particularly at the lower pressures (below 200 MPa), which may have been associated with splitting and cracking at the ends. The turnover in the curves at higher pressures probably represents bulging or buckling strains.

Rod A was used to span the pressure range 0.1 to 500 MPa to determine the general pattern of behaviour, and specimens from rods B and C were deformed mostly at pressures below 100 MPa to provide more data in the lower range, where the pressure sensitivity of strength appeared to be higher than at higher pressures. All specimens tested below 100 MPa pressure failed by longitudinal splitting (brooming), or by crushing at the ends involving longitudinal splitting, in contrast to the well developed kinking at high pressures (Fig. 1).

The relationship between confining pressure and strength for rod A is plotted in Fig. 3 (closed points). Here there appears to be a linear relationship between pressure and strength, with perhaps some unusually wide scatter of results below 100 MPa. The slope of this curve, by best-fit methods, was unity (Table I), which suggests a direct effect of pressure on strength; the zero pressure strength was 556 MPa.

Because of the large scatter of results at low pressures three or four specimens of rods B and C were deformed at each pressure level and six

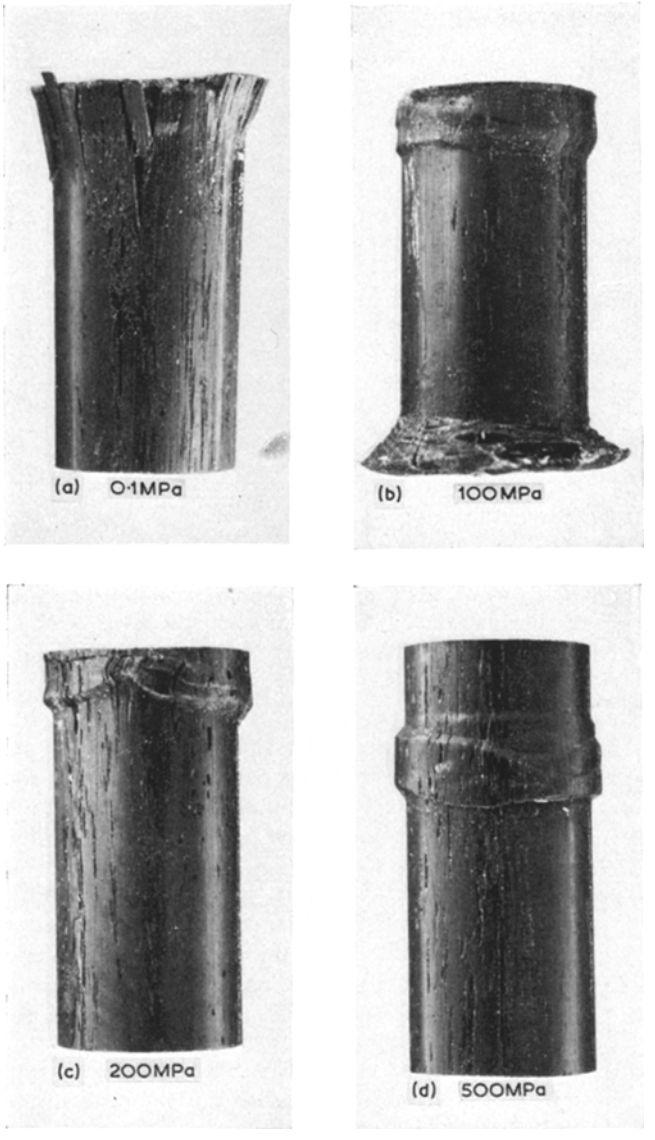

Figure 1 Compression tests on carbon–epoxy composite showing the changes in deformation behaviour under increasing hydrostatic pressures. Compression axis vertical, × 5.

TABLE I

Pressure range (MPa)	Zero pressure strength (MPa)	Slope of line (ψ)
0–100	511	3.2
100–500	556	1.0

at atmospheric pressure. These results are shown as scatter bars with a mean value indicated, in Fig. 4. A linear relationship again appears to exist up to 80 MPa, a best fit curve being drawn in Fig. 4. Here the slope was much higher than in Fig. 3 ($\psi = 3.2$) and the zero pressure strength was lower (510 MPa) as shown in Table I.

At high pressures, however, test results on rods B and C coincided well with the data from rod A (open circles, Fig. 3) at 400 and 500 MPa pressure, suggesting that the lower slope at high pressures was common for the three rods.

Figs. 3 and 4 suggest that two different mechanisms of failure operate in the high and low pressure ranges, and it is clear that the low pressure mechanism is much more sensitive to the application of the confining pressure than the high pressure mechanism.

3.2. Microscopical examination of deformation structures

The deformed structures in the specimens were

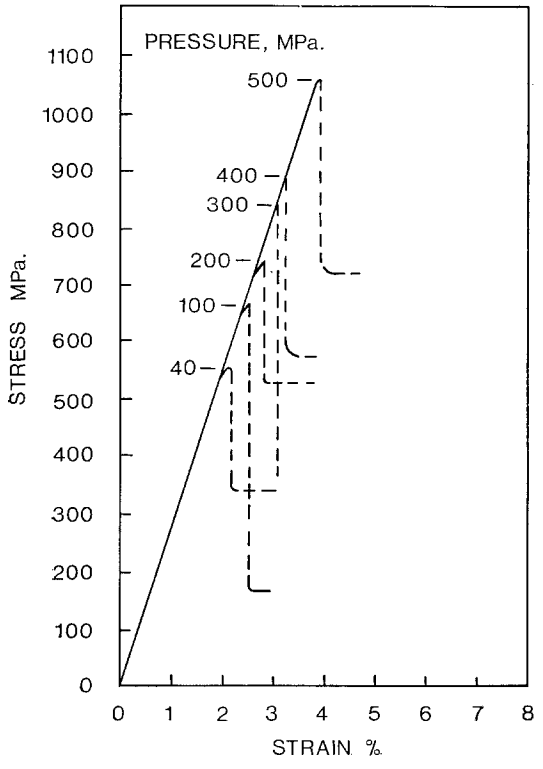

Figure 2 Nominal stress–strain curves for carbon–epoxy composite deformed in compression under high hydrostatic pressure.

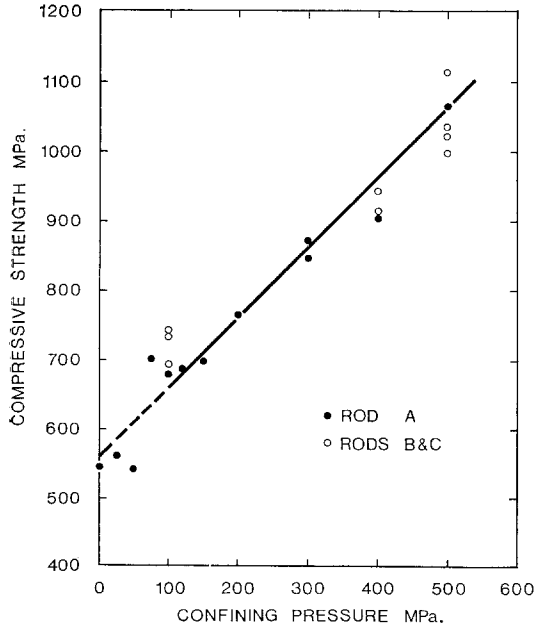

Figure 3 Effect of hydrostatic pressure on the strength of carbon–epoxy composite.

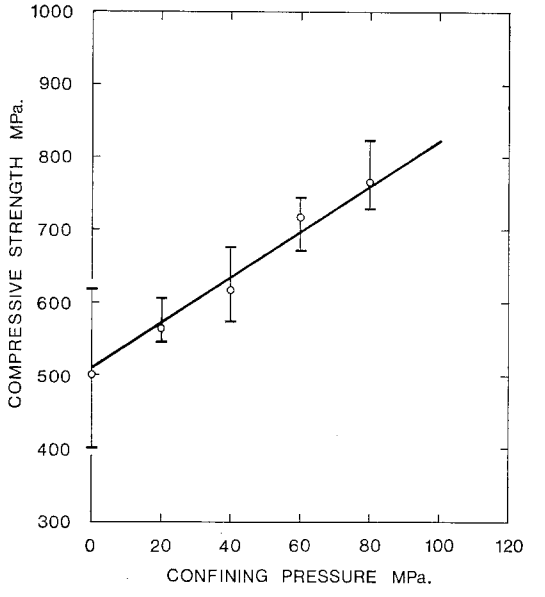

Figure 4 Effect of hydrostatic pressure up to 100 MPa on the strength of carbon–epoxy composite. Rods B and C.

examined by preparing polished cross-sections for examination under the optical microscope. These sections were prepared by mounting the specimens in epoxy resin and grinding away the specimen and mount on SiC papers in a plane parallel to the longitudinal axis of the specimen. The final surfaces were prepared by standard metallographic methods, using fine SiC abrasive papers and finishing on a 0 to 1 μm grade diamond abrasive pad. This presented a highly polished section in which, with care, most of the carbon fibres were retained intact as shown in Figs. 5 to 8, where the carbon fibres appear white. The original structure of the composites consisted of fairly parallel arrays of continuous fibres held in an epoxy matrix, as shown in the undamaged areas of Figs. 5 to 8. Misorientation was generally small, except for a few strands, but occasional channels of fibre-free epoxy matrix were found in most of the sections examined (e.g. Fig. 6).

Fig. 5 shows the microstructure of a longitudinal section of a specimen deformed at atmospheric pressure. Failure was by longitudinal splitting and brooming at one end (Fig. 1a), but in the body of the specimen, the microstructure contained evidence of more widespread damage. Longitudinal cracks at the fibre-matrix interface were frequently present (Fig. 5), denoting areas of failure under the transverse

Figure 5 Microstructure of a longitudinal cross-section of a carbon–epoxy composite deformed at atmospheric pressure, showing evidence of longitudinal fracturing (cf. Fig. 1a). Compression axis vertical, × 500.

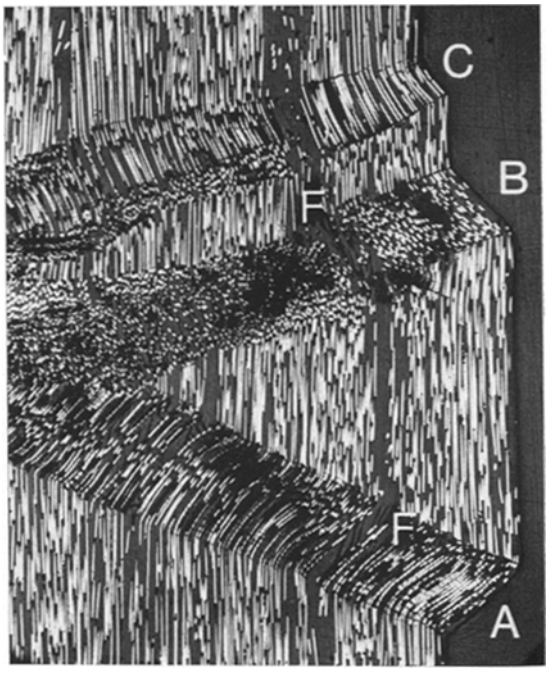

Figure 6 Microstructure of a longitudinal section of the kinked regions of a carbon–epoxy composite deformed at 500 MPa pressure (right-hand side of section) (cf. Fig. 1d). Compression axis vertical, × 37.

tensile stresses. It was difficult to prevent these cracked regions from breaking away during mechanical polishing, and many long fissures were produced where lengths of fibre and resin had fallen out.

Such cracking and loss of material from the section during polishing was rare in specimens deformed at high pressures, in the regions remote from the kinks (see Figs. 6 and 8) although parts of the heavily fractured kinked regions did break away (e.g. kink A, Fig. 6). Longitudinal cracking and production of fissures during polishing were considered to be more characteristic of specimens deformed at atmospheric pressure.

Fig. 6 shows a longitudinal section of a specimen deformed at 600 MPa pressure (Fig. 1d), in which the kinked structures were best developed. This specimen contained a pair of conjugate kinks which traversed the specimen and intersected on the longitudinal axis. Fig. 6 shows the right-hand half of a diametral section of the kinked region, in which the conjugate kinks are marked A and B. A third kink, C, lies

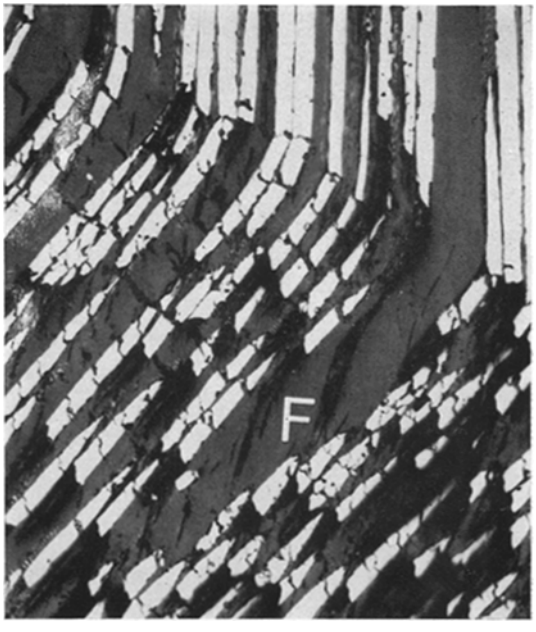

Figure 7 Microstructure of kink A showing broken C fibres and cracks in the epoxy matrix. Compression axis vertical, × 240.

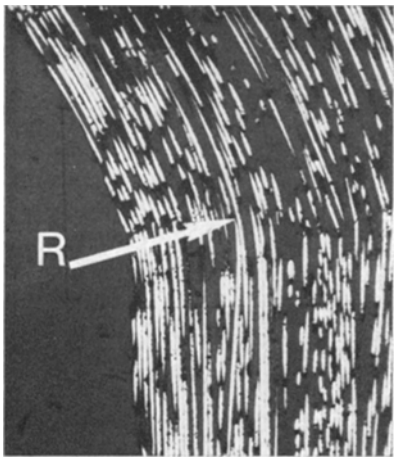

Figure 8 Microstructure of a longitudinal section of a bent region of a kinked carbon–epoxy composite (Fig. 1d) adjacent to kink B, left-hand side of specimen. Bent fibre indicated by arrow. Compression axis vertical, × 75.

parallel to kink B but stops in the body of the specimen and does not penetrate the other kinks. The kink band boundaries are defined by arrays of fractures in the fibres where a sharp change of orientation occurs.

These kinks illustrate different features of deformation. In kink A the fibres lie principally parallel to the plane of the section and the band boundaries are defined by lines of transverse fractures in the fibres. In addition, however, these fibres are broken into a series of short lengths of remarkably consistent periodicity, as illustrated at high magnification in Fig. 7.

In kink B, the direction of rotation of the fibres is opposite to that in A, and hence tends to restore the relative positions of the two ends of the specimen. Kink B was not co-planar with A because the axis of rotation of the structure was skew to the plane of the section. The fibres, therefore, appear as elliptical sections.

The fibres in kink C also lie almost wholly parallel to the plane of the section, but consist of almost complete and unbroken lengths within the kink band. We consider that this is not a primary kink as A and B are, but was probably formed later to accommodate the large lateral strains in the specimen introduced by the constraints of the deforming pistons on the ends. Klassen-Neklyudova *et al.* [7] have shown that, during the kinking process in compression, the specimen is very severely bent and warped and rocks about violently, while the ends remain relatively fixed. The speed of propagation of the kink can also be high, and rates of 2 m sec^{-1} have been estimated [7]. The bending which occurs adjacent to the kinking regions causes fractures in the fibres, to form a broad kink as in C, in which long lengths of unbroken fibres persisted, unlike the progressive fracturing by which the primary kinks A and B developed. Fig. 7 also contains evidence of fracturing of the epoxy within the kinks. These cracks usually arose from the fractures in the fibres, but others appeared to develop from internal strains, as discussed in Section 4.2.3.

In regions adjacent to the kinks, zones of severe bending sometimes developed, as in Fig. 8. These formed a transition zone between the unstrained parts of the specimen and the kinks, and were usually filled with long lengths of broken fibres. Occasionally, however, fibres remained completely unbroken, as at *R* in Fig. 8, providing a measure of the elastic bending of the fibres which could occur before fracture, as discussed in Section 4.2.2. We can thus distinguish two types of behaviour, which coincide to a large extent with the two different slopes of the pressure–strength curves in Figs. 3 and 4.

At low pressures, the composites failed by longitudinal splitting, apparently caused by failure of the interfacial bond between fibre and epoxy (Fig. 1a); this caused large pieces of fibre to fall out of the polished sections of the specimens, as shown in Fig. 6, and corresponds to the region of high slope of the pressure–strength curve at low pressures.

At high pressures, failure occurred by kinking. Longitudinal splitting was suppressed, and there was no evidence of interfacial failure in the body of the specimen away from the kinks. Within the kink bands also, the fibres usually remained firmly attached to the epoxy resin, and failure occurred by bending and breaking of the fibres. Here the slope of the pressure-strength curve is lower, approximately unity, i.e. the strength of the composite increased in direct proportion to the increase of applied confining pressure.

4. Discussion

4.1. The geometry of kinking

It is frequently stated that composites fail, when loaded in compression parallel to the fibre axis, by shearing in a plane lying at about 45° to the direction of the applied stress, near the plane of maximum resolved shear stress [3, 8]. The detailed mechanism of failure to be proposed

here, however, involves buckling of the fibres and/or kinking. We have no evidence in the present high pressure experiments that shear bands formed in or near the planes of maximum resolved shear stress; moreover, there is no evidence of shear failure. The mechanism of transverse deformation observed is clearly that of kinking, where shear takes place initially in a direction parallel (or at a high angle) to the principal stress axis (and parallel to the fibre axis in these specimens). This movement follows from the fundamental geometry of kinking, and is found to be common to many materials, including ductile crystalline materials [9], brittle crystalline materials and metamorphic rocks [10], linear structures such as timber, and even telephone books [11]. Similar deformation by kinking has been noted in polyester resin reinforced with soft steel wires [8].

Kink bands form in composite structures when they are deformed in compression in a direction parallel to the direction of greatest strength. In crystalline structures this would be parallel to the easy glide plane with the slip direction normal to the principal stress axis [9], but in composite structures and laminar structures the direction will be more or less parallel to the foliation or layering of the structure. Kinks form by rotation of parallel lamellae of approximately equal thickness away from their original position, as illustrated in Fig. 9. For geometrical reasons, involving the strain-energy of the system [12], the axes of rotation of the lamellae or "packets" (marked A in Fig. 9) are parallel and lie on a common plane which forms the kink band boundary (KBB) or plane of kinking. For similar geometrical reasons the plane of the KBB bisects the angle between the original direction of the structure and the "kinked" structure. During the development of the kink, the kink band boundary therefore moves from a position lying *normal* to the direction of shear in the lamellae, and rotates in the same sense or direction as the lamellae in the kink band, but at half the rate, as shown in Fig. 9.

Shear within the kinking structure, therefore, begins in a direction *normal* to the kink band boundary, not parallel to it, although the rotation of the lamellae may produce lateral displacements. The kink bands then develop diagonally across the specimen but not, however, parallel to the direction of maximum resolved shear stress, (which lies at 45° to the principle stress axis). The KBB usually lies at an angle

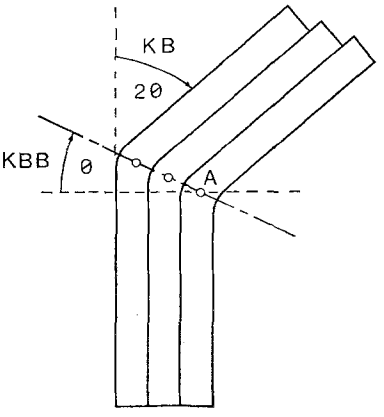

Figure 9 Geometrical elements of a kink band. A is the axis of rotation of the lamellae and 2θ is the angle of rotation of the structure in the kink. Compression axis vertical.

which seldom exceeds 30° to the normal to the principal stress axis, and in the present specimens these angles did not exceed 26° (Table II).

The rotations of the fibres in the kink bands A and C, Fig. 6, conform to these geometrical constraints, as shown in Table II.

TABLE II Angles of kink bands and boundaries

	Kink band*	Boundary+
Kink A	50°	26°
Kink C	44°	22°

*Angle between fibre and vertical axis (the axis of principal stress).
+Angle between KBB and normal to axis.

It should also be noted that the kink band boundaries in specimens deformed under high pressure appear quite planar, and that the conjugate kinks shown in Fig. 6 were typical of the kinking which takes place in specimens deformed in compression when strongly constrained at the ends [7].

It is also a characteristic of kinking that it develops from elastically or plastically buckled systems and that in anisotropic materials the slenderness ratio at which buckling failure occurs on a macroscopic scale is reduced to quite small ratios [12]. The buckling theories of failure in composites, as developed by Rosen [1, 2] and others [13, 14] are, therefore, not incompatible with the development of kinking, and we have examined the present experimental results in the light of buckling theory.

4.2. A model for kinking

At atmospheric pressure, the concept of micro-buckling provides the basis for models of failure of fibre-reinforced composites under compressive loading [1, 2, 13, 14]. Where buckling occurs in opposite senses, the extension or tensile mode of failure can occur which produces longitudinal splitting [1, 2] and, when co-ordinated buckling of fibres all in the same direction occurs, the "shear mode" develops which produces lateral displacements. Unless special precautions are taken to suppress splitting, e.g. by specially shaping the specimen, or, as in the present experiments, by applying a high confining pressure, failure in compression frequently occurs by splitting at the ends (brooming) and collapse of the exposed fibres, with large areas of decohesion between matrix and fibre (see Figs. 1a and 5). Hence, in this case, the strength of the composite, ultimately depends on its transverse strength, principally as determined by the matrix. At high confining pressures, however, the incidence of longitudinal splitting is prevented by the applied normal confining stresses, and buckling of the fibres can develop to a stage where major deformation bands, in the form of kinks, develop transversely across the specimen.

Microscopical examination of longitudinal sections of the kinked composites (Figs. 6 to 8) reveals two interesting features.

(1) In the primary kink A (Fig. 6), the fibres were broken into quite short lengths along almost the whole of their length within the kink band. This feature is illustrated more clearly in Fig. 7.

(2) In other parts of the specimen, evidence of fibres which were strongly bent but still unbroken was found, as shown in Fig. 8.

These observations provide an opportunity for testing current theories of buckling and the strength of composites against the experimental measurements.

4.2.1. Buckling of carbon fibres

In the simplest case, the fracture of the brittle carbon fibres in the kinks (e.g. kink A, Figs. 6 and 7) can be assumed to result from simple Eulerian buckling of a beam on an elastic foundation [1, 2, 15] following which, at a limiting surface strain, the buckled lengths break in half, as postulated by Berg and Salama [1, 5]. The load and the wave-form of the buckle would then be transferred along the fibre (by the lateral displacement of the next part of the fibre in the buckle) and the process repeated, so that a series of fractures would develop along the length of the fibre.

The length of buckled fibre, l which would be produced by an applied axial stress, σ_f, on the fibre is given by the Euler equation as follows:

$$\sigma_f = \frac{\pi^2 E_f}{(l/K)^2} \text{ or } l = \pi k \sqrt{\left(\frac{E_f}{\sigma_f}\right)}.$$

At 500 MPa pressure, the composite kinked at an axial force of 1010 MPa, which represents a stress on the fibres of $\sigma_f = 3000$ MPa, since the fibres occupied only about 36% of the area. Assuming that the epoxy matrix contributed little to the strength, and taking $E_f = 260$ GPa, the fibre diameter $d = 6.8 \times 10^{-3}$ mm and the radius of gyration $k = d/4 = 1.7 \times 10^{-3}$ mm, the length of buckled fibre in the kink would be 5×10^{-2} mm.

The average length of broken fibre in kink A was 2×10^{-2} mm. Since these fractured lengths represent half the total buckled length, the buckled lengths in the microstructures would have been about 4×10^{-2} mm, which is in reasonable agreement with the calculated value.

The buckled length, l, however, is a relatively insensitive parameter of strength, since it varies only with $\sqrt{(1/\sigma_f)}$. Thus, at atmospheric pressure ($\sigma_f = 1530$ MPa) $l_0 = 7 \times 10^{-2}$ mm and, conversely, the theoretical stress corresponding to a buckled length of 4×10^{-2} mm would be 4500 MPa (composite strength 1600 MPa) or 50% higher than that determined experimentally.

4.2.2. Elastic bending of carbon fibres

Associated with the kinking are zones of continuously curved structure which act as a transition between parts of the kinked zones and the undeformed parts of the specimens [9]. Within this curved zone, many fibres are broken into long lengths, but occasional fibres remain intact, as shown in Fig. 8. Here the radius of curvature, R, of the unbroken fibre was 0.53 mm. Assuming each fibre was strained equally in tension and compression about its neutral axis ($\epsilon_t = \epsilon_c$), the elastic strain at the surface would be

$$\epsilon_t = \epsilon_c = d/2R \text{ whence } \epsilon_t = 0.65\%.$$

A similar elastic strain is derived from the failure stress in the fibre obtained from the mixture rule

$$\sigma_f = \frac{\sigma_c - \sigma_m(1 - V_f)}{V_f}.$$

At zero pressure σ_c = 550 MPa, σ_m = 1.5 MPa [16] and V_f = 0.36, whence σ_f = 1525 MPa. This corresponds to an elastic strain in the fibres of σ_f/E_f or 0.6% strain. Since the limiting elastic strain in these fibres is less than 1%, it is evident that the fibres (Fig. 8) were held in a position of nearly maximum strain by the general strain in the matrix. If some elastic recovery took place following removal of the applied axial load, then even higher elastic strains would have been sustained during kinking.

These observations strongly support the view that kinking is initiated by buckling of the fibres, and that the kinks propagate by successive buckling and fracture of the fibres (not necessarily involving fracture of the matrix).

4.2.3. Cracking in the epoxy

Shearing strains develop during rotation and growth of the lamellae to form the kink band, introducing elastic and plastic strains in the epoxy matrix of the lamellae. When the strains are large, as in broad bands of unreinforced matrix, tensile fracturing occurs as seen in Figs. 6 and 7 (in both kinks A and B, marked F). It was not possible to determine whether these cracks developed during or after kinking under pressure under load, or whether they opened up after removal of the load and pressure by relief of internal strains. The direction and position of these arrays of parallel cracks in the epoxy matrix of the kink band, however, which were not connected with the fibre fracturing process, is evidence of the large strains involved in kinking.

The cracks in the carbon fibres frequently extended a short distance into the matrix (Fig. 7), sometimes to the extent of joining up with cracks in adjacent fibres particularly where the fibres lay very close together. There was, however, no evidence of longitudinal fracturing of either the fibre-epoxy interface or of the fibres themselves. The fibres outside the kinks, in the undeformed matrix, remained completely unfractured in these high pressure specimens.

4.2.4. Kinking

The model for kinking now proposed involves the buckling of fibres on an elastic foundation in the composite in a Eulerian manner. Some of the fibres become bent to a critical strain and fracture, and the kink then grows in an axial direction (broadens) from a small nucleus of broken fibres by this process, and at the same time spreads across the width of the specimen by transfer of load to adjacent fibres which were already buckled by the axial strain. The orientation of the kink band boundary also moves (rotates) simultaneously away from its original transverse position and becomes tilted towards the axis of principal stress [9].

All this would happen very rapidly during the time the applied axial force was falling during yielding (Fig. 2) and the process would stop when the applied force had fallen to a level where buckling or bending of the unbroken fibre outside the kink was insufficient to cause fracture. The strong lateral displacement caused by the growth of one kink band would be opposed by the restraints at the ends of the specimen, causing a complementary kink to form in the opposite sense. In this way a pair of conjugate kinks would form, as illustrated in Fig. 6. Compensatory bending adjacent to these kinks would produce regions of bent fibres (Fig. 8) or secondary kinks outside the main kink bands (kink C, Fig. 6).

4.3. Strength and pressure

4.3.1. Failure criteria

The Rosen theory of buckling failure [1, 2] has been widely accepted as a model for compressive failure of composites, particularly when the ratio of the elastic moduli of the fibre and matrix exceeds 120 [4], as in the present composite in which $E_f/E_m \simeq 160$.

Calculations of the theoretical failure stress σ_{ct} for the tensile mode in this composite predicts far too high a strength, however:

$$\sigma_{ct} = \frac{2V_f^{2/3}\sqrt{(E_m E_f)}}{3(1 - V_f)}$$

whence σ_{ct} = 15 GPa, compared with the measured failure stress at atmospheric pressure of only 0.55 GPa.

The shear mode of failure [1, 2] is concerned principally with the properties of the matrix:

$$\sigma_{cs} = \frac{G_m}{1 - V_f}$$

whence

$$\sigma_{cs} = 0.95 \text{ GPa}$$

which accords better with the experimental failure stress of about 0.55 GPa at atmospheric pressure. Introduction of the "effective" shear modulus 0.63 G_m to allow for non-planar buckling [17] reduces σ_{cs} to 0.6 GPa, in good agreement with experiment. This shear model,

however, takes no account of either the strength of the fibre or of the large effects of pressure on strength and, for the case of strong fibres in a stiff matrix, models based on Eulerian buckling [13-15] appear more relevant.

4.2.3. Strength and pressure

On the basis of the Rosen shear model, we would expect that the strength of the composite would vary only with the elastic modulus of the matrix (G_m), since the elastic strength of the carbon fibres would not be expected to be influenced by the moderate confining pressures applied. The elastic modulus and failure strength of the epoxy itself have been found to increase slightly under pressure [16], but not enough to explain the increase in strength of the composite. The elastic modulus of the epoxy increases by only 35% between atmospheric and 500 MPa pressure, and the elastic limit (at 2% strain) by 30% [16]. Since the contribution of the epoxy to the strength of the composite was only 2 to 3 MPa [16] in the 500 MPa measured at atmospheric pressure, the pressure-strengthening of the epoxy would have had little influence on the strengthening of the composite.

Strengthening effects under pressure would, however, arise in part from the influence of the hydrostatic confining pressure acting directly as a normal stress component across the fracture surfaces, and in part from the resolved component of maximum principal stress, according to the Mohr theory, as follows [18]

$$\sigma_n = \sigma_3 + (\sigma_1 - \sigma_3) \sin^2 \theta$$

where θ is the angle between the plane of the fracture and the direction of the maximum principal stress. The resolved tangential forces are smaller and less dependent on confining pressure:

$$\tau = (\sigma_1 - \sigma_3) \sin \theta \cos \theta .$$

Here, $(\sigma_1 - \sigma_3)$ is the differential stress component of the maximum principal stress, which represents the non-hydrostatic axial stress in the material being deformed.

Unfortunately, the angle θ which the plane of fracture originally makes with the direction of the principal stress is uncertain, due to the buckling of the fibres and the development of the structure in the kink bands. These angles may be estimated directly, however, from the experimental plots of Figs. 3 and 4, through the relationships [18]

$$\theta = \frac{\pi}{4} - \frac{\phi}{2}$$

and

$$\tan \phi = \frac{\tan \psi}{2(1 + \tan \psi)^{\frac{1}{2}}} .$$

The slopes of the curves in Figs. 3 and 4 are $\tan \psi_H = 1$ and $\tan \psi_L = 3.16$ respectively. These curves represent only the stresses on the whole composite, however, assuming the carbon fibres carry the whole of the applied force, the true slopes are $\tan \psi / V_f$ where the volume fraction of fibres $V_f = 0.36$; whence the values given below are obtained.

Pressure range (MPa)	$\tan \psi$	$\tan \phi$	$\phi°$	$\theta°$
0–100 (L)	8.7	1.4	54.5	18
100–500 (H)	2.8	0.72	36	27

At pressures over 100 MPa, the calculated angle of fracture $\theta_H = 27°$ does not coincide with the angle of the kink band boundaries ($\theta_{KBB} = 64°$, Fig. 3). It thus appears that the geometrical requirements for kinking operate independently of the fracture angle in the individual fibres, and that the buckled fibres initially fracture at an effective angle of less than 30° to the principal stress axis. The fibres in the kinks then become displaced and the planes of fracture move towards the principal stress axis as seen in Fig. 7.

The very high pressure sensitivity of strength below 100 MPa pressure can be similarly ascribed to the low angle of fracture (nominally 18°), which would correspond to longitudinal tensile fracturing of the fibre–matrix interface in the buckled condition (Fig. 5).

These results suggest that the longitudinal splitting which occurs in unidirectional composites deformed in compression parallel to the fibres could be offset by some lateral constraint. The lateral strains represented by elastic bulging of the composite under load introduce transverse tensile forces. In the present experiments these strains would not be affected by the high confining pressures, but the propagation of internal cracks would be inhibited.

In a fabricated body, however, structural members under compression would require the lateral strains to be reduced mechanically, in order to reduce the magnitudes of transverse tensile forces. This could be done by introducing short fibres lying transversely to the main fibre

axis, or perhaps by using circumferential windings in which the tensile hoop stresses would have a similar effect.

5. Conclusions

The application of confining pressures of about 100 MPa or higher changes the failure mode of carbon-epoxy composites deformed in compression from longitudinal tensile fracturing to kinking transversely across the specimen.

Kinking was initiated by the transverse fracture of buckled fibres. Propagation of the kink nucleus through the composite proceeded by a process of successive buckling and fracture along the fibres and in adjacent fibres to broaden the kink band and achieve propagation across the section.

The strength of the kinked composites correlated better with a model of simple Eulerian buckling on an elastic foundation than with theories based on the strength of the matrix. At high pressures, strength increased in direct proportion to the applied pressure.

Failure at low pressures appeared to be associated with tensile failure of the carbon-epoxy interface (following buckling of the fibres) and was much more sensitive to pressure than was the kinking stress.

References

1. B. W. ROSEN, "Mechanics of Composite Strengthening", A.S.M. Seminar, Phil. Pa. (October 1964).
2. *Idem*, Mech. Comp. Met. Proc. 5th Symp. Naval Structural Analysis (May 1967) p. 621.
3. NARMCO R & D DIV. WHITTAKER CORP., Contract AF 33 (615)-1660, AFML TR 65-237 (May 1965).
4. O. ORRINGER, ASOFR Sci. Rep., ASRL TR 162-1 (Oct. 1971).
5. H. C. HEARD, *J. Geology* **71** (1963) 162.
6. M. S. PATERSON, *Int. J. Rock. Mech. Min. Sci.* **7** (1970) 517.
7. M. V. KLASSEN-NEKLYUDOVA, M. A. CHERNYSHEVA and G. E. TOMILOVSKII, *Sov. Phys. – Cryst.* **5** (1961) 617.
8. E. M. DE FERRAN and B. HORNES, *J. Comp. Mats.* **4** (1970) 62.
9. E. OROWAN, *Nature* **149** (1942) 643.
10. M. S. PATERSON and L. E. WEISS, *Geol. Soc. Amer. Bull.* **77** (1966) 343.
11. L. E. WEISS, Proceedings of the Conference on Research in Tectonics, Ottawa 1968, Paper No. 68-32, edited by A. J. Baer and D. K. Morris (Geol. Survey Canada, 1969) p. 294.
12. J. B. HESS and C. S. BARRETT, *Trans. Met. Soc. AIME* **185** (1949) 599.
13. L. R. HERRMAN, W. E. MASON and S. T. K. CHAN, *J. Comp. Mats.* **1** (1967) 212.
14. Y. LANAIR and Y. C. B. FUNG, *ibid* **6** (1972) 387.
15. C. A. BERG and M. SALAMA, *Fibre Sci. Tech.* **6** (1973) 79.
16. C. W. WEAVER and J. WILLIAMS, to be published.
17. J. R. LAGER and R. R. JUNE, *J. Comp. Mats.* **3** (1969) 48.
18. C. B. RALEIGH and M. S. PATERSON, *J. Geophy. Res.* **70** (1965) 3965.

Received 31 December 1974 and accepted 10 January 1975.